Supplementary Data

Table S1: Data collection and refinement statistics

Data collection	Apo	Zn
Space group	$P2_122_1$	$P2_122_1$
Cell dimensions		
a, *b*, *c* (Å)	86.05, 92.42, 116.73	86.06, 91.85, 115.93
α, β, γ (°)	90, 90, 90	90, 90, 90
Resolution (Å)	50 – 2.5	50 – 3.0
R_{sym}	5.4 (64.2)	10.2 (53.8)
$I / \sigma I$	34.5 (3.6)	10.6 (2.1)
Completeness (%)	100.0 (100.0)	91.4 (94.0)
Redundancy	7.8 (8.0)	4.3 (4.4)
Refinement		
Resolution (Å)	50.0 – 2.5	50 – 3.0
No. reflections	33,330	29106
R_{work} / R_{free}	23.9 / 25.9	24.4/ 27.4
No. atoms		
Protein/DNA	7,000	7,000
Ion	0	8
Water	113	20
Average B-factor (Å^2)		
Protein/DNA	78.4	88.9
Ion	n/a	123.0
Water	47.7	53.0
R.m.s. deviations		
Bond lengths (Å)	0.009	0.007
Bond angles (°)	1.2	1.2

*Values in parentheses refer to the highest-resolution shell.

Supplementary Fig. Legends

Fig. S1 – DNA bending parameters

As indicated under all three graphs, the DNA substrate contains a 3'-bridging phosphorothiolate between the -1 thymine (red, boxed) and the +1 cytosine. Two complementary strands (bottom) adjoin at a nick (red arrowhead). Blue diamonds indicate where the DNA bends.

a Base pair rise. The average rise of B-form DNA (3.2 Å) is indicated by the dotted line.

b Base pair roll.

c Base pair twist. The average twist of B-form DNA (36°) is indicated by the dotted line. Each panel was made using the output of 3DNA[42].

Fig. S2 – Comparison of the topo II active site with classic two-metal enzyme systems

a Superposition of the covalent-complex active site (cyan/green/yellow) with ribonuclease H (RNaseH, dark blue) bound to uncleaved RNA[43]. The two magnesium ions seen in RNaseH (blue spheres) straddle the scissile phosphate; one resides close to the metal A position seen in the topo II model (black spheres).

b Superposition of the covalent-complex active site (cyan/green/yellow) with the BamHI restriction endonuclease (pink) bound to cleaved DNA products[44]. As with RNaseH, both metal ions (pink spheres) straddle the scissile phosphate; again, one is situated in a position analogous to metal A (black spheres) in the present structure.

Fig. S3 – Alignment of active site residues for type IA topoisomerases

The presence of a conserved lysine in the type IA topoisomerase active site is highlighted in red. The lysine alternates between two adjacent positions between topo I (TopA) and topo III (TopB) paralogs. The metal A-binding glutamic acid is highlighted in cyan. *E. coli* amino acid numberings are indicated.

Fig. S4 – Type IIA topoisomerase gating motions

a Stereo image superposing the winged helix domains for the covalent-complex structure (magenta) on the prior non-covalent structure (cyan)[13]. Movement of the active site tyrosine is enabled by an inward rocking of the WHD.

b Alignment of the salt-bridge network that links active site status to C-gate dynamics. Although the alignment initially suggests that two positions are not strictly conserved in some bacterial type IIA topoisomerases (the aspartate in *E. coli* topo IV and one of the two arginines in *M. tuberculosis* gyrase), inspection of structural models available for these outliers shows that the salt bridge connection is actually maintained by compensatory mutations in nearby residues (shaded letters, see also panel c).

c The salt-bridge networks in *E. coli* topo IV (ParC, *left*, salmon) and *M. tuberculosis* gyrase (GyrA, *right*, pale green). Compare to Fig. 4b in the text.

d Comparison of DNA-gate transitions in the principal DNA binding ("A′") region of type IIA topoisomerases. (*Left*) DNA-gate "closed." The present topo II cleavage complex is shown in cyan, with the TOPRIM domains removed for clarity. (*Right*) DNA-gate "open." An apo structure of yeast topo II (PDB ID 1BGW)[27] is shown with the TOPRIM domains removed for clarity. In both instances, the C-gate interface is closed, and constitutes the primary means through which the protein dimerizes.

Fig. S5 – Model for the relative timing of gate opening and closing during the type II topoisomerase reaction

In all panels, a green circle denotes a cleaved G-segment or open C-gate, while a red octagon denotes a locked (closed) gate. Three dissociable interfaces – the N-gate (upper yellow domains), DNA-gate (middle blue/cyan region with purple cylinder) and C-gate (lower blue "tips") – control G-segment cleavage and T-segment transport in response to ATP binding and hydrolysis. Although the exact timing of gate opening and closure has not been determined experimentally, available structural information shows that the C-gate can spontaneously open upon G-segment

binding, even when no T-segment is present[13]. By contrast, the status of the C-gate appears closed when: 1) the enzyme is not bound to DNA and the DNA gate is shut[28,45], 2) the enzyme is not bound to DNA and DNA gate is open[27,29,46], or 3) the enzyme is bound to DNA, but the duplex is cleaved (as seen in the present study and elsewhere[47].) These observations are consistent with a mechanism in which G-segment binding allosterically destabilizes the C-gate, shifting the status of the interface from a predominantly associated form to one that can open and close with frequency. The likelihood of the C-gate opening would be adjusted (to a more or less favorable event) depending on the state of the topoisomerase reaction.

(1) A G-segment DNA (purple) is bound and bent at the DNA gate. The C-gate is destabilized and now capable of opening, but trends toward a closed state.

(2) ATP binding dimerizes the ATPase domains (the N-gate, yellow) capturing a T-segment (green). The G-segment DNA is cleaved, with the positioning of the active-site tyrosine ensuring that the C-gate is locked shut.

(3) The DNA gate is opened, allowing T-segment passage. The C-gate remains closed.

(4) The DNA-gate closes and configures the active site for G-segment religation.

(5) Religation and loss of the tyrosine-DNA link allosterically frees the C-gate to open, an event that may be favored by the presence of the T-segment resident between the interfaces.

Fig. S6 – Modeling of alternate DNA half sites

a $2F_o$-F_c maps showing representative electron density (1 σ contour) around positions T_{+6}/A and A/T_{-2} base pairs (see Fig. 1b for numbering) highlights the averaged features of the DNA resulting from the operation of the crystallographic dyad.

b Same as (a), but showing composite simulated-annealing omit maps at 1 σ contour.

Supplemental Movie SM1

The transition between cleaved and uncleaved DNA states permits C-gate opening. The movie begins with the reported structure (3L4J), colored as in Fig. 1c. The structure then morphs into a non-covalent structure with the C-gate open (2RGR)[13]. The catalytic tyrosine is shown in red. Intermediate states used to make the movie were modeled using CNS[48] and software written by the Yale Morph Server[49]. Images were generated using PyMol[39], and the movie was compiled using Quicktime Pro (Apple).

Fig. S1

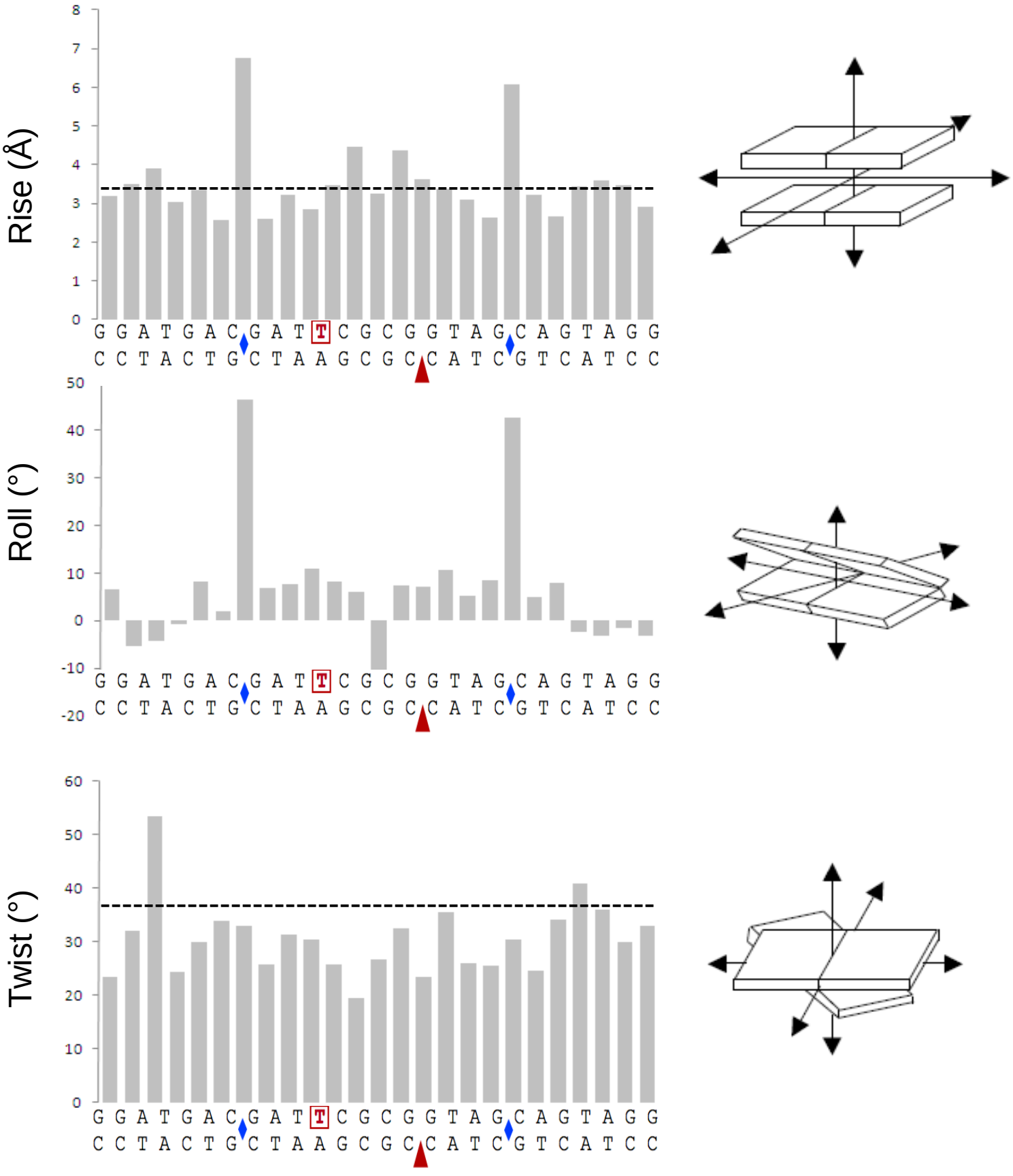
Rise (Å)
8
7
6
5
4
3
2
1
0
G G A T G A C G A T T C G C G G T A G C A G T A G G
C C T A C T G C T A A G C G C C A T C G T C A T C C
Roll (°)
50
40
30
20
10
0
-10
-20
G G A T G A C G A T T C G C G G T A G C A G T A G G
C C T A C T G C T A A G C G C C A T C G T C A T C C
Twist (°)
60
50
40
30
20
10
0
G G A T G A C G A T T C G C G G T A G C A G T A G G
C C T A C T G C T A A G C G C C A T C G T C A T C C

Fig. S2

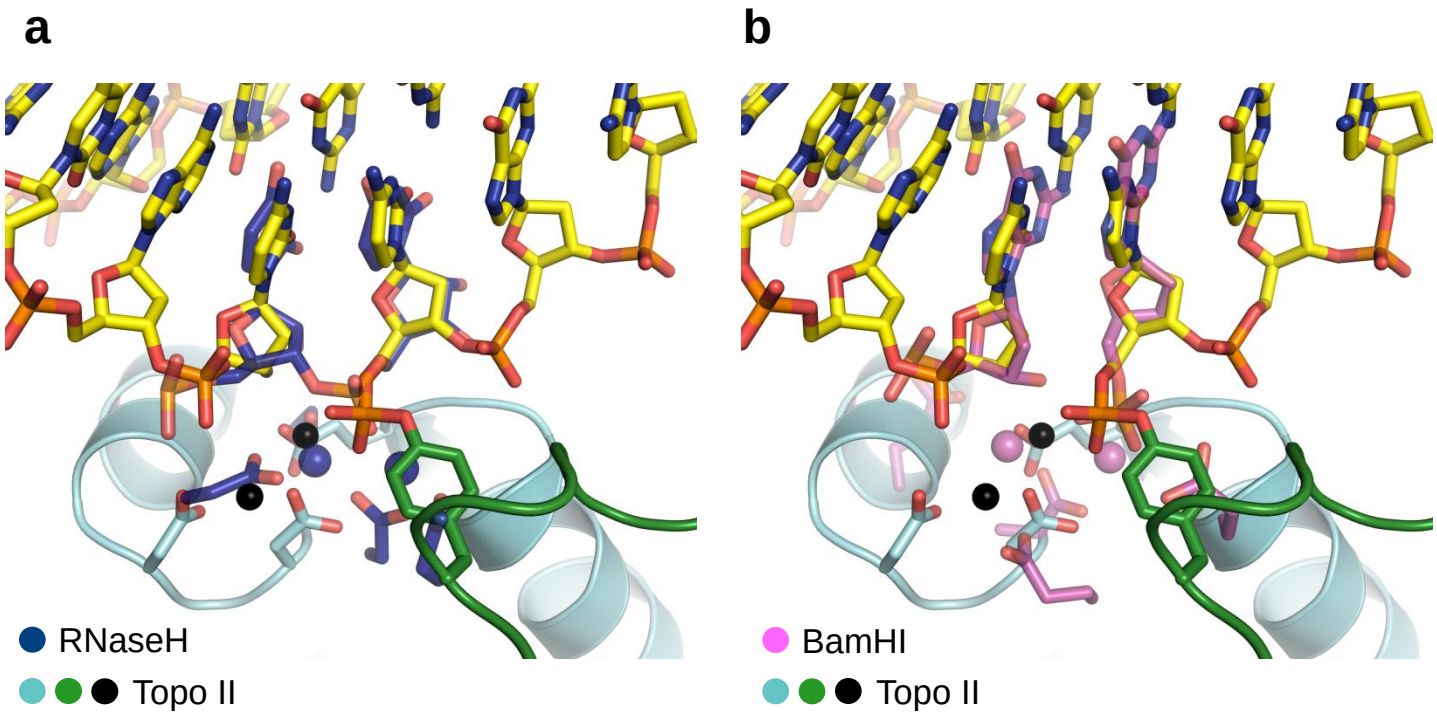

Fig. S3

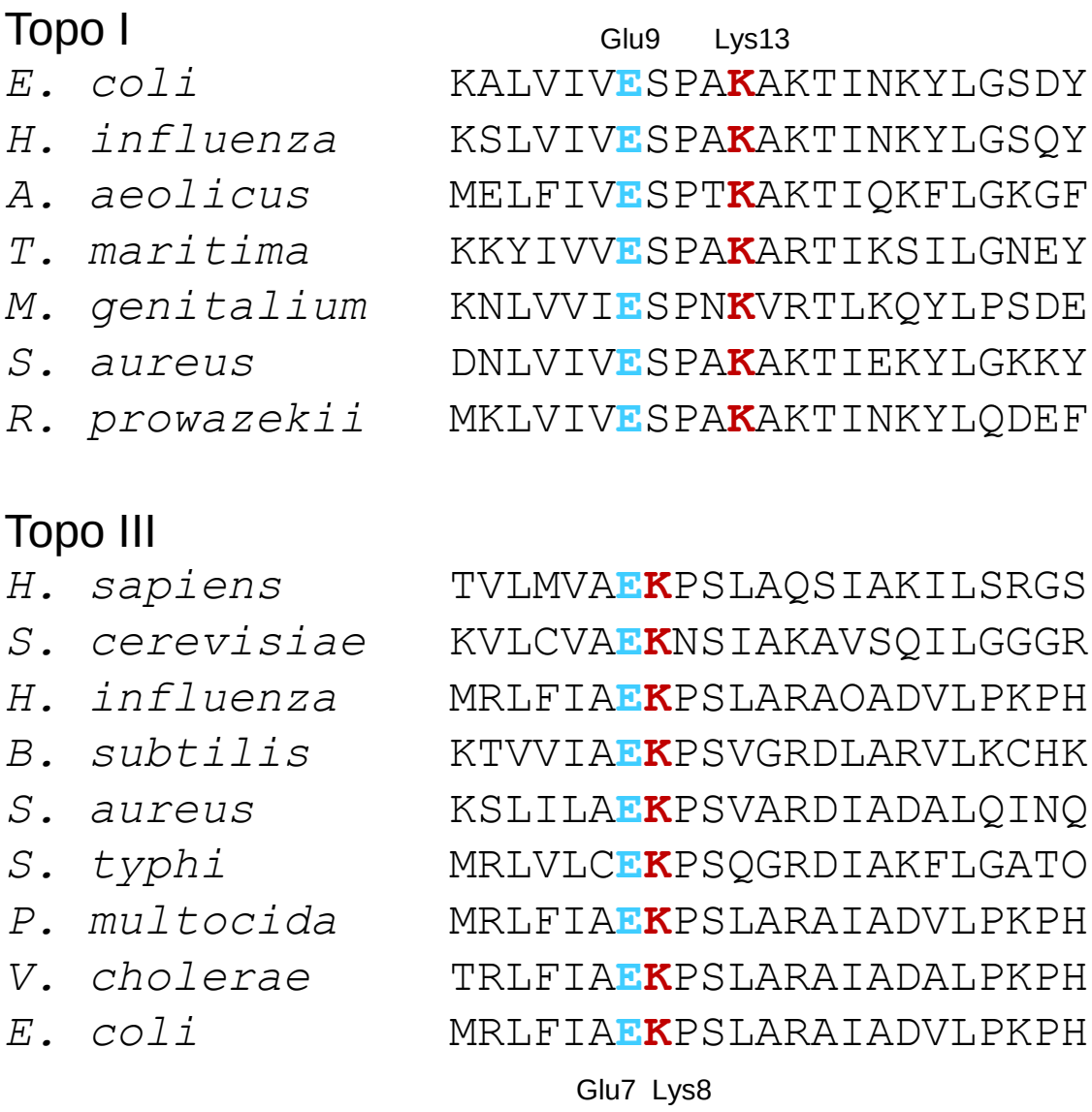
Topo I
Glu9
Lys13
E. coli KALVIVESPAKAKTINKYLGSDY
H. influenza KSLVIVESPAKAKTINKYLGSQY
A. aeolicus MELFIVESPTKAKTIQKFLGKGF
T. maritima KKYIVVESPAKARTIKSILGNEY
M. genitalium KNLVVIESPNKVRTLKQYLPSDE
S. aureus DNLVIVESPAKAKTIEKYLGKKY
R. prowazekii MKLVIVESPAKAKTINKYLQDEF
Topo III
H. sapiens TVLMVAEKPSLAQSIAKILSRGS
S. cerevisiae KVLCVAEKNSIAKAVSQILGGGR
H. influenza MRLFIAEKPSLARAOADVLPKPH
B. subtilis KTVVIAEKPSVGRDLARVLKCHK
S. aureus KSLILAEKPSVARDIADALQINQ
S. typhi MRLVLCEKPSQGRDIAKFLGATO
P. multocida MRLFIAEKPSLARAIADVLPKPH
V. cholerae TRLFIAEKPSLARAIADALPKPH
E. coli MRLFIAEKPSLARAIADVLPKPH
Glu7 Lys8

Fig. S4

a

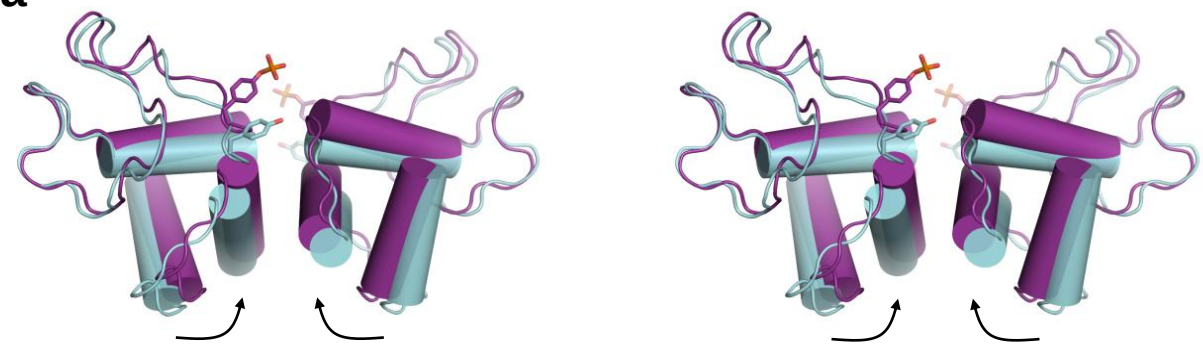

b

		Asp799
Top2	*S. cerevisiae*	TELNKLTRKIFHPA**D**DPLYKYI
Top2	*S. pombe*	TALSPLARVLFNSN**D**DQLINYQ
Top2α	*Human*	TMLSSLARLLFPPK**D**DHTLKFL
Top2	*Mouse*	TMLSPLARLLFPPK**D**DHTLRFL
Top2	*Drosophila*	TIMSPLTRLIYHPL**D**DPLLDYQ
Top2	*Arabidopsis*	TKLSPVTRILFPKD**D**DLLLDYL
GyrA/B	*E. coli*	IRLAKIAHELMA**D**LEKETVDFV
GyrA/B	*A. aeolicus*	AKLSPLAVEMLT**D**IDKDTVDFQ
GyrA/B	*M. tuberc.*	ARLTPLAMEMLR**E**IDEETVDFI
ParC/E	*E. coli*	SRLSKYSELLLS**E**LGQGTADWV

		Arg1001	Arg1008
Top2	*S. cerevisiae*	EFYYV**R**LEYYQK**R**KDHMSERLQ
Top2	*S. pombe*	EFYEV**R**LRTYQR**R**KEHMVNELE
Top2α	*Human*	DFFEL**R**LKYYGL**R**KEWLLGMLG
Top2	*Mouse*	DFFEL**R**LKYYGL**R**KEWLLGMLG
Top2	*Drosophila*	EYYKL**R**REYYAR**R**RDFLVGQLT
Top2	*Arabidopsis*	EFFDL**R**FEYYEK**R**KETVVKNME
GyrA/B	*E. coli*	AFVRH**R**REVVTR**R**TIFELRKAR
GyrA/B	*A. aeolicus*	EFIKH**R**LEVILR**R**SKYFLKKVQ
GyrA/B	*M. tuberc.*	YYVDHQLDVIVR**R**TTY**R**LRKAM
ParC/E	*E. coli*	EWLVF**R**RDTVRR**R**LNYRLEKVL

Fig. S4

c

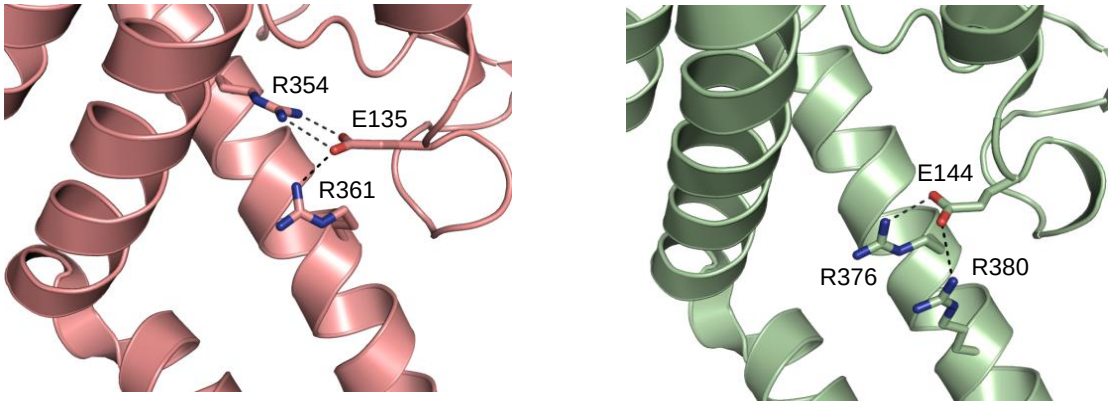

d

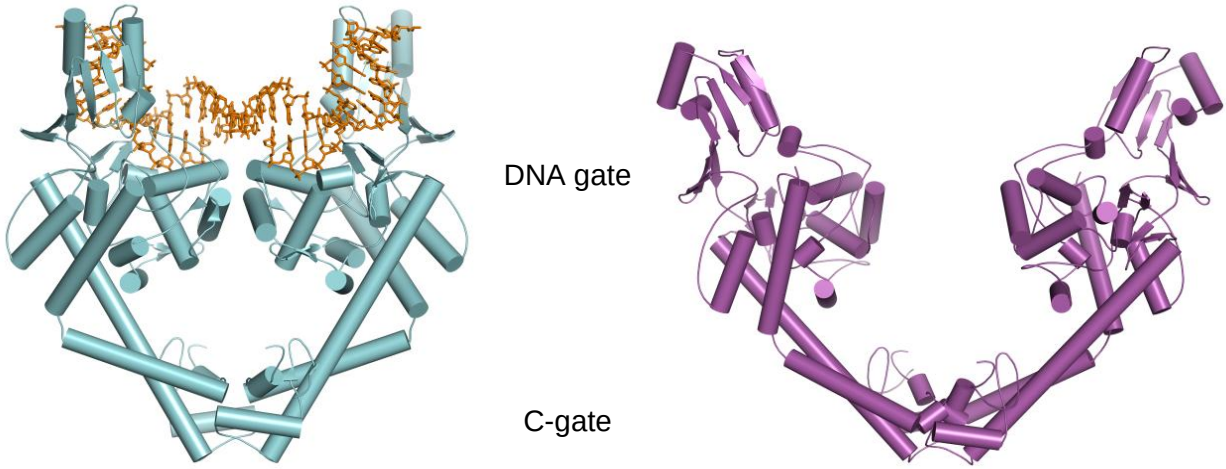

Fig. S5

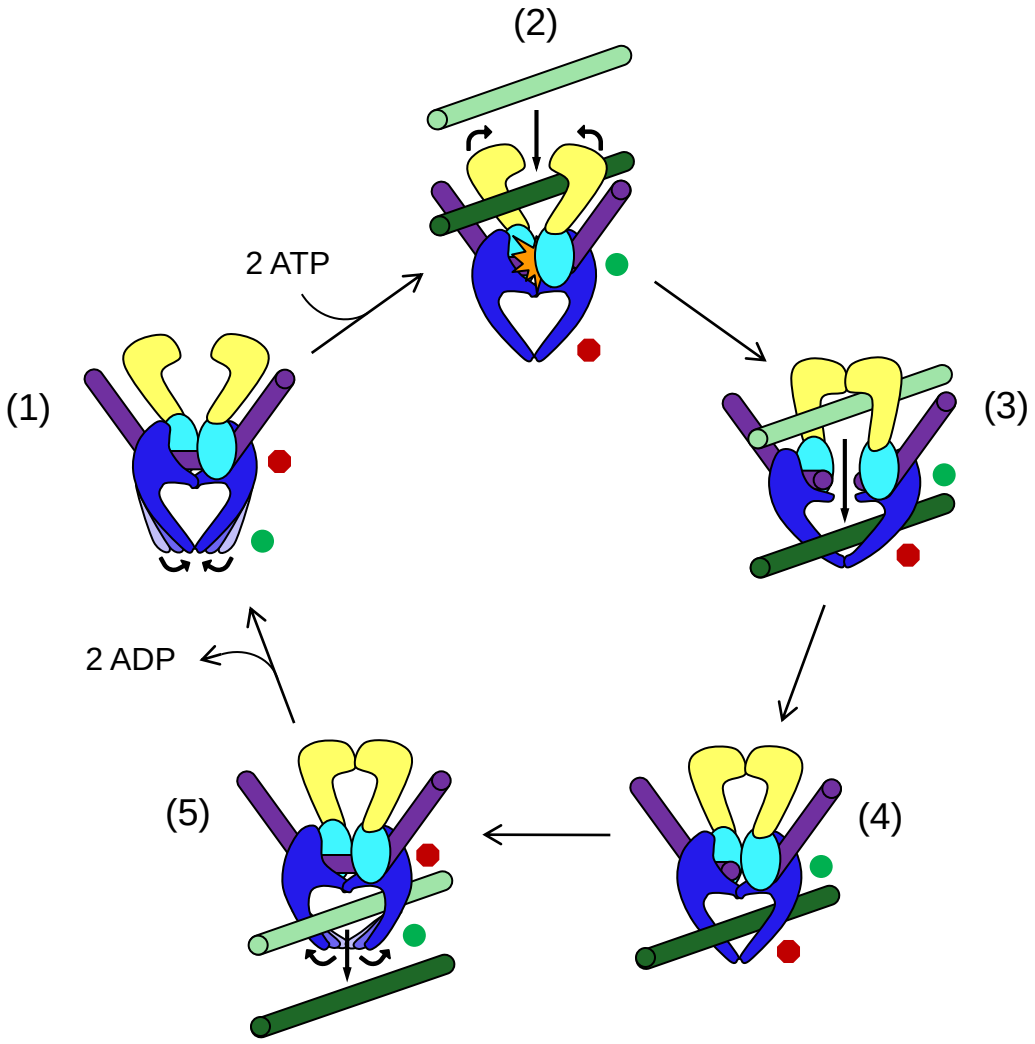

	(1) G-segment binding	(2) G-segment cleavage	(3) T-segment transport	(4) G-segment religation	(5) T-segment release
DNA gate	Closed	Closed	Open	Closed	Closed
C-gate	Open → Closed	Closed	Closed	Closed → Open	Open

Fig. S6

a

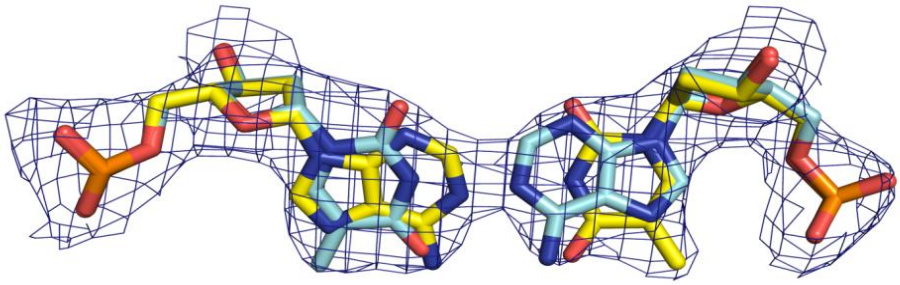

b

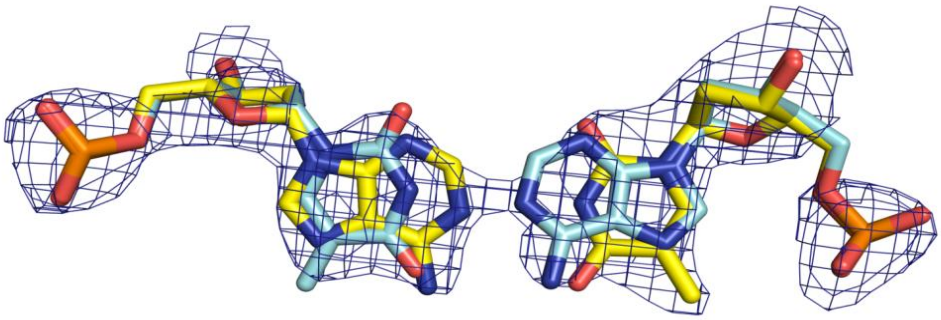

References

42. Lu, X.J. & Olson, W.K. 3DNA: a versatile, integrated software system for the analysis, rebuilding and visualization of three-dimensional nucleic-acid structures. *Nat Protoc* 3, 1213-27 (2008).

43. Nowotny, M., Gaidamakov, S.A., Crouch, R.J. & Yang, W. Crystal structures of RNase H bound to an RNA/DNA hybrid: substrate specificity and metal-dependent catalysis. *Cell* 121, 1005-16 (2005).

44. Viadiu, H. & Aggarwal, A.K. The role of metals in catalysis by the restriction endonuclease BamHI. *Nat Struct Biol* 5, 910-6 (1998).

45. Tretter, E.M., Schoeffler, A.J., Weisfield, S.R. & Berger, J.M. Crystal structure of the DNA gyrase GyrA N-terminal domain from Mycobacterium tuberculosis. *Proteins* 78, 492-5.

46. Corbett, K.D., Schoeffler, A.J., Thomsen, N.D. & Berger, J.M. The structural basis for substrate specificity in DNA topoisomerase IV. *J Mol Biol* 351, 545-61 (2005).

47. Laponogov, I. et al. Structural insight into the quinolone-DNA cleavage complex of type IIA topoisomerases. *Nat Struct Mol Biol* 16, 667-9 (2009).

48. Brunger, A.T. Version 1.2 of the Crystallography and NMR system. *Nat Protoc* 2, 2728-33 (2007).

49. Flores, S. et al. The Database of Macromolecular Motions: new features added at the decade mark. *Nucleic Acids Res* 34, D296-301 (2006).